

pubs.acs.org/JPCC Perspective

# Homogeneous Optical Line Widths in Hybrid Ruddlesden-Popper Metal Halides Can Only Be Measured Using Nonlinear Spectroscopy

Ajay Ram Srimath Kandada,\* Hao Li,\* Eric R. Bittner,\* and Carlos Silva-Acuña\*



Cite This: J. Phys. Chem. C 2022, 126, 5378–5387

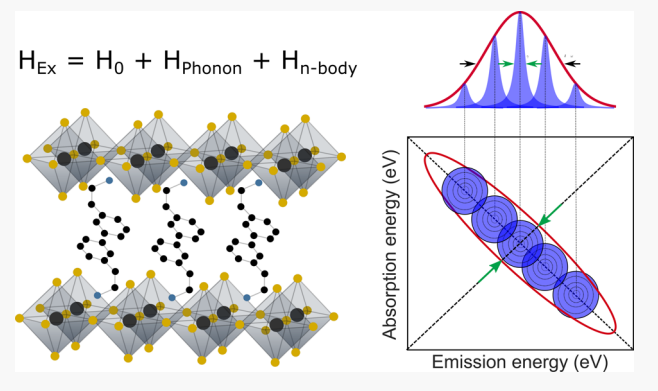


**ACCESS** I

III Metrics & More

Article Recommendations

ABSTRACT: The homogeneous photoluminescence spectral line width in semiconductors carries a wealth of information on the coupling of primary photoexcitations with their dynamic environment as well as between multiparticles. In the limit in which inhomogeneous broadening dominates the total optical line widths, the inhomogeneous and homogeneous contributions can be rigorously separated by temperature-dependent steady-state photoluminescence spectroscopy. This is possible because the only temperature-dependent phenomenon is optical dephasing, which defines the homogeneous line width, since this process is mediated by scattering with phonons. However, if the homogeneous and inhomogeneous line widths are comparable, as is the case in hybrid Ruddlesden—Popper metal halides, the temperature dependence of linear spectral measurement *cannot* separate rigorously the



homogeneous and inhomogeneous contributions to the total line width because the line shape does *not* contain purely Lorentzian components that can be isolated by varying the temperature. Furthermore, the inhomogeneous contribution to the steady-state photoluminescence line shape is not necessarily temperature independent if driven by diffusion-limited processes, particularly if measured by photoluminescence. Nonlinear coherent optical spectroscopies, on the other hand, do permit separation of homogeneous and inhomogeneous line broadening contributions in all regimes of inhomogeneity. Consequently, these offer insights into the nature of many-body interactions that are entirely inaccessible to temperature-dependent linear spectroscopies. When applied to Ruddlesden—Popper metal halides, these techniques have indeed enabled us to quantitatively assess the exciton—phonon and exciton—exciton scattering mechanisms. Here, we will discuss our perspective on how the coherent line shapes of Ruddlesden—Popper metal halides can be effectively rationalized within an exciton polaron framework.

#### INTRODUCTION

Two-dimensional (2D) hybrid Ruddlesden—Popper metal halides, colloquially referred to as 2D hybrid perovskites, are self-assembled and solution-processed semiconductors that have multiple quantum-well-like materials architectures and physical properties. Current interest in these materials stems from their strongly excitonic properties that arise from electronic and dielectric confinement in two-dimensional layers of metalhalide octahedra that are separated by long organic cations such as phenethylammonium or *n*-butylammonium. Strongly bound electron—hole pairs are thus observed in these materials and these are treated as Wannier—Mott excitons much like other two-dimensional semiconductors such as composite quantum wells and single-layer transition metal dichalchogenides.

Given the immense interest in these materials for optoelectronic technologies, including in emerging quantum optoelectronics, where coherent properties of optical excitations play a primary role, quantifying the many-body interactions of excitons is extremely relevant. This includes measurement of exciton—phonon coupling, elastic multiexciton scattering, and biexciton

binding energies. Linear optical spectroscopy, which measures the absorption, photoexcitation, or photoluminescence (PL) of the sample, is widely employed for that purpose. For example, the temperature dependence of the PL line width is routinely analyzed to obtain the energy and coupling coefficients of phonons that scatter the excitons.<sup>4–7</sup> The density dependence of the PL spectra is considered to be an estimate of the biexciton binding energies.<sup>8</sup> It must be noted, however, that these methodologies have been developed decades back mainly for epitaxially grown II—VI quantum wells and other similar systems, which exhibit very low energetic disorder.<sup>9,10</sup> Rigorous analysis of the PL line shapes has severe limitations even in such

Received: January 27, 2022 Revised: March 8, 2022 Published: March 22, 2022





systems due to many-body effects and nontrivial inhomogeneous contributions that arise in any ensemble measurement. Such contributions are even more dominant in solution-processed, self-assembled systems such as metal-halide hybrids. Moreover, the existence of additional dynamic disorder effects from the organic—inorganic interactions 11 and a strongly anharmonic lattice with substantial electron—phonon coupling puts metal-halide perovskites within a much more complex scenario. In this manuscript, we provide pertinent arguments to show that linear spectroscopy of such material systems, widely employed in the community, provides incomplete and often incorrect information. This may lead the oversimplification of the rather complex and unique photophysics simply because the data *fit* to an established model.

Coherent nonlinear spectroscopy, <sup>12</sup> on the other hand, is a well suited technique not only to identify many-body interactions but also to perceive the mechanistic subtleties of the scattering processes. Here, we provide an extensive tutorial on the correlation between the coherent nonlinear spectral line shapes and the many-body interactions and how the various bath interactions can be systematically decomposed and measured on the basis of simple theoretical models. We will review two of our recent works (ref 13 and ref 14) on a prototypical Ruddlesden—Popper metal halide, and we discuss the insights gained on the fundamentally unique nature of the excitons in these material systems.

#### **■ EXCITON DEPHASING**

In condensed matter, the spectral line shape of an optical resonance encodes a wealth of information on the interactions of the system under investigation with its environment. The use of the spectral line width in atomic, molecular, and semiconductor spectroscopies as a quantitative probe of system-bath interactions is extensively employed. The underlying physical principle behind this methodology has been first formulated by Anderson<sup>15</sup> and Kubo<sup>16</sup> within the framework of the stochastic scattering theory. In the single-particle Anderson-Kubo picture, the transition energy of the particle (an atom, a molecule, or an exciton in a crystal) is modulated by the stochastic fluctuations in its environment. These fluctuations may be driven by scattering processes involving phonons (or local vibrations), dielectric fluctuations, or multiparticle collisions (see Figure 1). The result is an intrinsic time dependence of the transition frequency  $\omega_{01}(t) = \omega_{01} + \delta \omega_{01}(t)$ , where  $\omega_{01}$  is the central frequency and  $\delta\omega_{01}$  is the modulation such that  $\langle\delta\omega_{01}(t)\rangle=0$ (see Figure 1a).

In a simple two-level system, the transition probability from the ground state,  $|0\rangle$ , to the first excited state,  $|1\rangle$ , is proportional to the off-diagonal element of the density matrix,  $\rho_{01}$ , which is also referred to as the coherence. In the absence of any perturbation to the system—bath Hamiltonian, the off-diagonal elements are zero. In other words, there is no projection of the ground state onto the excited state. An optical excitation induces a time-dependent component in the Hamiltonian:  $H_{\rm int}(t) = \vec{\mu} \cdot \mathbf{E}(t)$ , where  $\vec{\mu}$  is the transition dipole moment and  $\mathbf{E}(t)$  is the electric field of the optical excitation pulse. The coherence term will accordingly oscillate as shown in Figure 1b following eq 1:

$$\rho_{01}(t) = \rho_{01}(0) \exp\left(-i \int_0^t \omega_{01}(\tau) d\tau\right)$$
(1)

In an experiment, an ultrashort optical pulse excites an ensemble of particles with a well-defined phase coherence. However, with

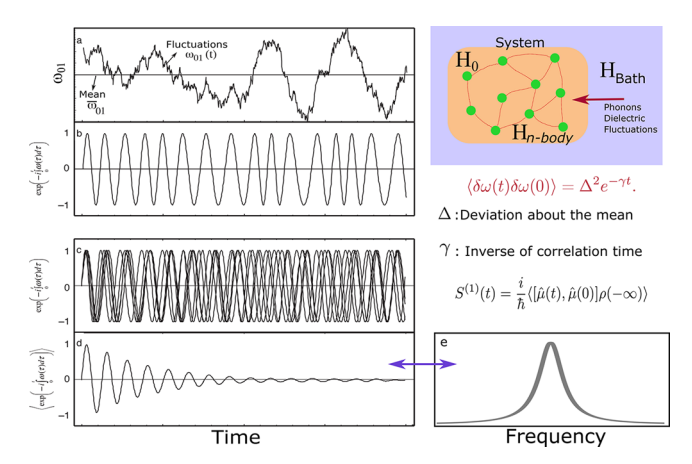


Figure 1. (a) Fluctuations in the exciton transition energy,  $\omega_{01}$ , around a mean value, driven by bath interactions, sketched on the right. (b) Value of the coherence term  $\rho_{01}$  of a single particle excitation with a time varying frequency due to the fluctuations. (c) Coherence terms of a ensemble of excitations created in phase by the optical pulse, which evolve differently due to the random fluctuations. (d) Time average of the coherence term, which decays due to the dephasing process and whose Fourier transform is given by (e), which has a Lorentzian line shape. Panels a–d reproduced with permission from ref 17. Copyright 2011 Cambridge University Press.

each particle's energy prone to statistically random fluctuations subject to the bath interactions, as shown in Figure 1c, the measurement will perceive a time average of density matrix,  $\langle \rho_{01}(t) \rangle$ . The overall result is that the photoexcitations go out of phase exponentially over a period of time, referred to as the **dephasing time**, and the amplitude of the time averaged coherence term tends to zero, as shown in Figure 1d. The first-order optical response will be directly proportional to  $\rho_{01}(t)$ , the Fourier transform of which will be a Lorentzian line shape, as in Figure 1e. The prevalence of such a line shape in an absorption or photoluminescence experiment, however, depends on the relative time scales of the fluctations.

In order to be more quantitative about these time scales, we introduce a frequency autocorrelation function,  $\langle \delta \omega(t) \delta \omega(0) \rangle$ , which is a function of the frequency deviation about the mean,  $\Delta$ , and a certain correlation time for the fluctuations,  $\tau_c = \gamma^{-1}$ :

$$\langle \delta \omega(t) \, \delta \omega(0) \rangle = \Delta^2 e^{-t/\tau_c}$$
 (2)

The dephasing time is related to the correlation time,  $T_2$  =  $(\Delta^2 \tau_c)^{-1}$ . Note that this formulation has no underlying assumption concerning the nature of the environmental fluctuations. If  $\Delta \gg \gamma$ , the fluctuations are relatively slow, enabling the system to sample a broad inhomogeneous distribution of environmental conditions. This condition does not result in the time-domain response shown in Figure 1d. Accordingly, the absorption/emission spectrum takes a Gaussian line shape whose width has no dependence on the correlation time but is rather limited by the width of the inhomogeneous distribution sampled; thus, the line shape does not carry any information on the bath interactions. On the other hand, if the fluctuations are rapid enough,  $\Delta \ll \gamma$ , in the motional narrowing limit, the line width becomes increasingly narrow and assumes a Lorentzian form where the homogeneous line width,  $\gamma = \tau_{\rm c}^{-1}$  is now directly related to the dephasing time and thus quantifies the system-bath interactions. An intermediate regime with comparable homogeneous and inhomegeneous contributions to the line width is possible in systems that are subjected to

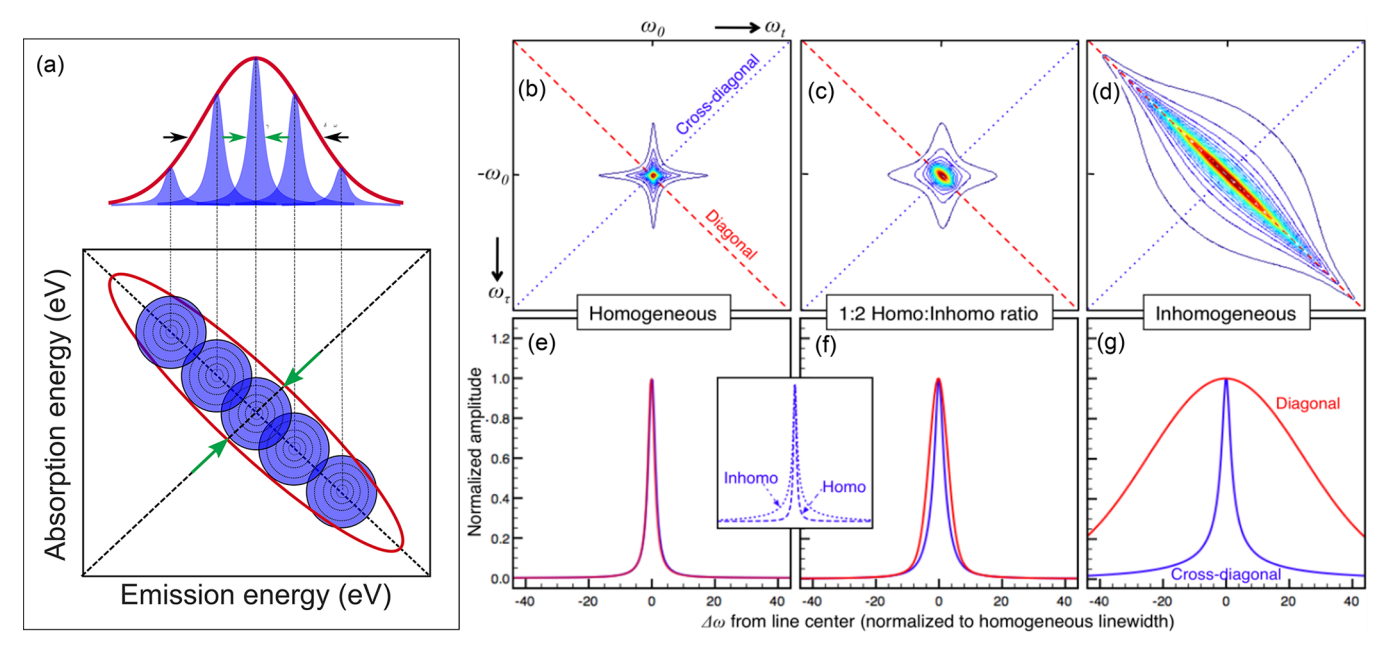


Figure 2. (a) Schematic representation of an inhomogeneously broadened Gaussian linear line shape, with a distribution of Lorentzian homogeneously boradened line shapes buried underneath it. In this scenario, the 2D coherent line shape reflects the inhomogeneous, Gaussian spectrum along the diagonal spectral cut, and the homogeneous, Lorentzian spectrum along the antidiagonal. The 2D coherent line shape is depicted in conditions of (b)  $\gamma \gg \Delta$  (homogeneous broadening), (c)  $\gamma \sim \Delta$  (moderate inhomogeneity), and (d)  $\gamma \ll \Delta$  (inhomogeneous broadening), along with corresponding diagonal and antidiagonal cuts in (e), (f), and (g), respectively. Panels (b)—(g) reproduced with permission from ref 18. Copyright 2010 The Optical Society.

static and dynamic disorder. We note that highly crystalline systems can also fall into this category subject to the inevitable disorder from the fabrication. <sup>18</sup> In such cases, the optical line shape has a much more complex behavior with the line width that is not directly correlated with the dephasing rate albeit being dependent on it.

Thermal Dephasing Probes. Of the various sources of environmental stochastic fluctuations, thermal excitation is a dominant one. Thermally populated vibrations, dielectric fluctuations, and in the case of crystals, phonons, scatter electronic excitations. This can be perceived as an increasing line width at higher temperature, and accordingly, it is common to analyze the temperature dependence of the linear spectral line widths measured via absorption or photoluminescence, to quantitatively estimate the electron—phonon coupling parameters. The homogeneous PL line width ( $\gamma$ ) is routinely modeled by assuming scattering of electrons with polar optical phonons and with long-wavelength acoustic phonons:

$$\gamma(T) = \gamma_0 + \alpha_{\rm ac}T + \alpha_{\rm opt}N_{\rm opt} \tag{3}$$

where  $\gamma_0$  is the temperature-independent, intrinsic line width, while  $\alpha_{\rm ac}$  and  $\alpha_{\rm opt}$  are the electron—acoustic phonon and electron—optical phonon coupling coefficients, respectively. The number of the optical phonons with energy  $E_{\rm LO}$  is  $N_{\rm opt}$  which is given by the Bose—Einstein distribution function,  $1/\left[\exp(E_{\rm LO}/k_{\rm B}T)-1\right]$ . It is worthwhile to note that this model has been developed primarily in the context of material systems fabricated with a low degree of disorder, such as epitaxial semiconductor quantum wells and quantum dots. This is evident from the reported line widths that are well below 10 meV (less than the relevant phonon energies) and the observed near-perfect Lorentzian spectral line shapes. However, there are still contributions from inhomegenous broadening effects due to measurable and unavoidable static disorder that limit application

of eq 3 even in these model material systems. While these contributions can be reduced via single-particle spectroscopy, they are inevitable in an ensemble measurement. In fact, the need to go beyond linear spectroscopies to measure true homogeneous line widths has been emphasized in several published works.  $^{18-20}$ 

Metal-halide perovskites and their derivatives exhibit PL line widths that are factors larger in magnitude than the relevant phonon energies with line shapes that are distinctly not Lorentzian. 4,6 This may be attributed fundamentally to their self-assembly process from solution, which is bound to generate substantial static morphological disorder. In addition, dynamic disorder is ubiquitous in the hybrid metal-halide lattice due to the independent motion of the organic cation. These sources of disorder inevitably increases the deviation in the frequency fluctuations, thus forcing the system to be in the limit where the line shape is an inhomogeneous distribution of homogeneously broadened transitions (see Figure 2a). The contributions of static and dynamic disorder are therefore comparable in these systems. In this condition, the PL line width is dominated by neither homogeneous nor inhomogeneous mechanisms, and eq 3 is not valid. In other words, the temperature dependence of the line width is not uniquely attributed to scattering with optical or acoustic phonons. Accordingly, the values of the coupling coefficients and phonon energies obtained from such an analysis, particularly in metal-halide perovskites, are at best upper bound estimates, and a direct measurement of the homogeneous line shape is necessary.

This model is yet widely used to derive very impactful conclusions on the photophysics of three-dimensional metal-halide perovskites, <sup>5,6</sup> hybrid layered metal halides (see refs 7 and 21–25 for a few examples), and nanostructured derivatives (for examples, see refs 26–30). While some of these published works qualitatively capture the nature of carrier—phonon and exciton—phonon interactions, none of the reported linear spectroscopies

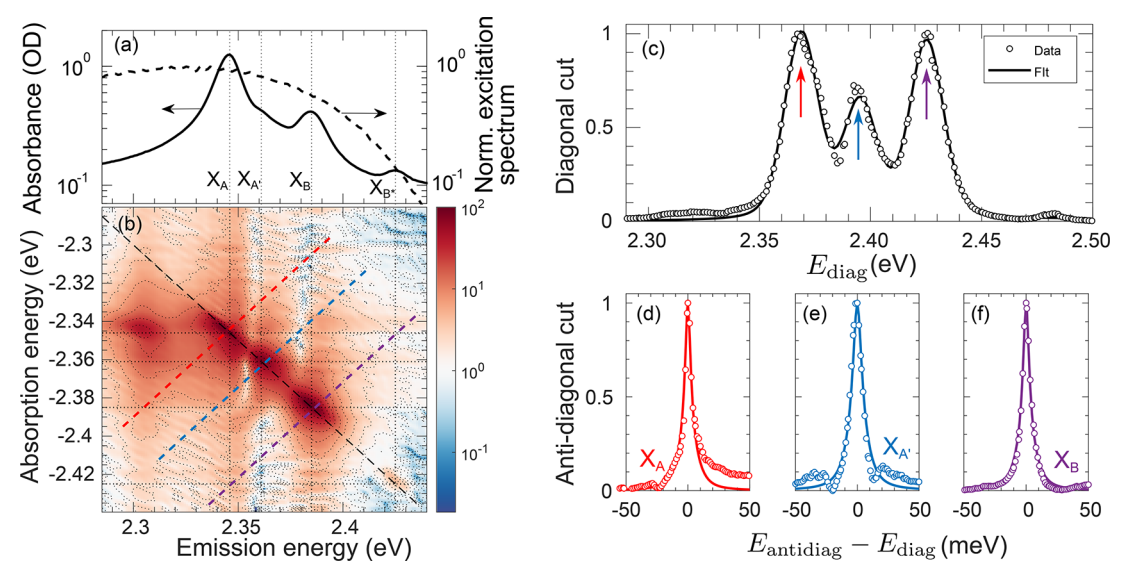


Figure 3. Linear and two-dimensional coherent spectroscopy of (PEA)<sub>2</sub>PbI<sub>4</sub> at 5 K. (a) Absorption spectrum of (PEA)<sub>2</sub>PbI<sub>4</sub> measured at 5 K (black line) and normalized spectrum of the pulses used in 2D coherent excitation spectroscopy measurements (dashed line). Both scales are logarithmic. Dotted lines indicate the energy of excitons A, A', B, and B\*, respectively, with increasing energy. (b) Absolute value of the 2D coherent rephasing spectrum of (PEA)<sub>2</sub>PbI<sub>4</sub> measured at 5 K with a pulse fluence of 40 nJ/cm² and a pump—probe delay of 20 fs. The color scale is logarithmic. Dotted lines indicate the energies of the aforementioned features. The paths of the diagonal cut (black dashed line) and antidiagonal cuts at the diagonal energy of excitons A, A', and B (red, blue, and purple dashed lines, respectively) are also shown. Reproduced with permission from ref 13. Copyright 2019 American Physical Society.

are able to provide quantitative estimates of the coupling coefficients by the arguments presented above. The insufficiency in this methodology is also evident in the wide variance in the reported phonon energies and coupling coefficients, with some of them estimating the relevant phonon energies to be above 50 meV, <sup>23,24</sup> factors above the rigorously estimated LO phonon energies of less than 10 meV in these material systems. <sup>31,32</sup>

One might argue that the inhomogeneous contributions to the line width can be modeled as a temperature-independent offset  $\gamma_0$  in eq 3. However, the photoexcitation can sample a broad range of site energies by diffusion processes that are temperature dependent and that happen within its lifetime. Thus, luminescence spectroscopy in particular, and any linear spectroscopy in general, is incapable of separating the fast dephasing dynamics and slow evolution of the population within the inhomegeneous energetic landscapes. Therefore, spectroscopic techniques that can *directly* distinguish between homogeous and inhomogeneous contributions to the total line width are required. Coherent multidimensional spectroscopy thus offers a viable alternative here, as demonstrated recently in refs 13, 19, and 33.

Two-Dimensional Coherent Optical Spectroscopy. In a two-dimensional coherent spectroscopy experiment, the nonlinear optical response of the sample is measured as a function of two independent energy (or frequency) variables.<sup>34</sup> The experiment itself involves photoexcitation of the sample with three phase-stabilized, ultrashort (typically ≤25 fs) optical pulses. The excitation geometry, commonly knowm as the boxCARS geometry, is such that each of the three pulses are at the vertices of a square while being focused onto the sample. The three optical pulse interaction induces a time-varying third-order polarization in the material that emits coherent radiation carrying the nonlinear material response. Due to the specific excitation geometry and the resulting phase-matching and time-ordering conditions, this signal is emitted along the fourth vertex of the square in the boxCARS geometry. The phase and

amplitude of the signal is then measured by interference with another low intensity optical pulse, a local oscillator with known phase and amplitude. The energy of the detected signal constitutes one of the axes of the two-dimensional spectrum and is referred to as the **emission energy** (see Figure 3b). Note that this is not the energy of the luminescence emitted by the photoexcited state via the population relaxation process, but it is the energy of the coherent signal emitted by the time-evolving coherent nonlinear polarization.

The second axis in the 2D correlation map, referred to as the **absorption energy**, is the energy at which the photoexcited population is created. This axis is constructed as the Fourier transform of the signal dynamics obtained by scanning the delay between the first two excitation pulses. Note that in a three-pulse excitation scheme, the first pulse creates a coherence like in eq 1 and the second pulse then projects the coherence onto a population, and the phase evolution of the signal between the first two pulses corresponds to the absorption event.

Figure 2a summarizes, albeit in a qualitative way, how a 2D coherent spectrum can separate inhomogeneous and homegeneous contributions, which manifest as diagonal and antidiagonal line widths, respectively. In the limit of motional narrowing ( $\Delta \ll \gamma$ ), however, there is no distinction between diagonal and antidiagonal line shapes, and the 2D spectrum is symmetric and *star-like*, as shown in Figure 2b. In the other extreme limit of inhomogeneous broadening ( $\Delta \gg \gamma$ ), the difference between the diagonal and antidiagonal line widths is evident (see Figure 2d) and  $\gamma$  can be estimated from the latter. In the intermediate regime ( $\gamma \sim \Delta$ ), like in the case of Ruddlesden–Popper metal halides and other metal-halide perovskite derivatives,  $^{7,13,14,32}_{,13,14,32}$  diagonal and antidiagonal widths depend on both  $\gamma$  and  $\Delta$ , and both line shapes become coupled as shown in Figure 2c.

In a such a scenario, a global fitting routine based on analytical expressions for the line shapes derived by Cundiff and coworkers 18 must be employed to quantitatively estimate the

homogeneous line width. There are additional experimental considerations based on the sequence of the optical pulses, phase-matching conditions, and appropriate population waiting times that enable true estimation of the homogeneous line width. While more extensive treatments can be found elsewhere, 17,34 it can be shown that the absolute value of the rephasing spectrum that is collected at (or close to) the zero population waiting time is the correct spectrum to be used in the analysis. The rephasing spectrum refers to the experimental condition in which the first pulse interacting with the sample is the one at the diagonally opposite vertex to the detecting local oscillator pulse in the boxCARS geometry. The rephasing signal is also referred to as the photon echo generated through a four wave mixing mechanism. We note that while there are other relatively simple experimental implementations of the 2D coherent spectroscopy,<sup>12</sup> some of them are not capable of measuring reliable homogeneous line widths due to their inability to isolate the coherent excitation pathways that give the appropriate total nonlinear response. It is important to underline that only the rephasing coherent pathway can quantitatively resolve the homogeneous contributions to the total coherent line shape under general conditions.

Measurement of Homogeneous Line Widths in (PEA)<sub>2</sub>Pbl<sub>4</sub>. A representative zero-time rephasing 2D spectrum of a prototypical Ruddlesden-Popper metal halide taken at 5 K is shown in Figure 3b. It must be noted that the spectral response at zero population time may be affected by the presence of coherent artifacts and pulse-ordering ambiguities. We exclude such contributions to the measured spectrum, on the basis of the consistent time evolution of the spectral line shape, which we discuss in refs 13 and 14, and we will come back to these dynamics later in this manuscript. We can identify three features along the diagonal corresponding to the three resonances in the linear spectrum in Figure 3a that correspond to the distinct excitonic states. 7,35,36 The 2D line shape clearly represents the intermediate condition of Figure 2c, and we performed a global fit of the diagonal (Figure 3c) and antidiagonal cuts (Figure 3df). We estimated comparable homogeneous and inhomogeneous line widths for this particular spectrum to be approximately 2.3 and 6.5 meV, respectively.<sup>13</sup>

The homogeneous line width is strongly dependent on both the excitation fluence and the sample temperature owing to the many-body exciton interactions, as shown in Figure 4. The line width increases linearly with increasing excitation density owing to exciton—exciton scattering, <sup>13</sup> also referred to as the excitation-induced dephasing (EID), with the slope of the curve quantifying the strength of such interactions. <sup>20</sup> It is notable that the strength of the interexciton interactions is distinct for each of the observed resonances. We will discuss the nature of EID later in this Perspective while noting the evolution of the 2D line shape with the population waiting time.

The thermal dephasing of the excitons, on the other hand, can be perceived by the temperature dependence of the line width. Having separated homogeneous and inhomogeneous contributions rigorously, eq 3 can now be reliably used to analyze this data set. We obtain good fits with the LO phonon scattering model for each of the observed resonances within the spectral fine structre at the exciton energy labeled  $X_{\rm A}$  and  $X_{\rm B}$  (see the last section of this Perspective for more discussion), and we estimate the energy of the phonon(s) participating in the elastic scattering process and the value of the exciton—phonon coupling coefficient. The thermal dephasing of exciton  $X_{\rm A}$  indicates that it is scattered by a LO phonon at 6.5 meV, <sup>13</sup>

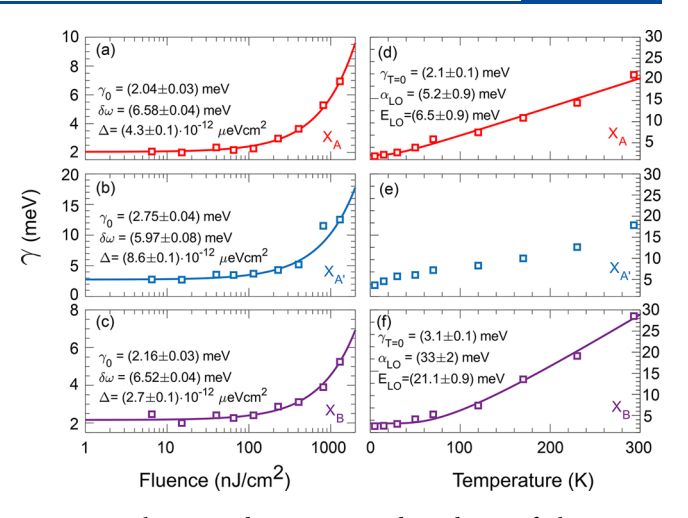


**Figure 4.** Fluence and temperature dependence of the exciton dephasing rates. Dephasing parameters  $\gamma$  of excitons A, A', and B (panels a and d, b and e, and c and f, respectively) obtained from the simultaneous fitting of diagonal and antidiagonal cuts, plotted as a function of excitation fluence (panels a–c) or temperature (panels d–f). Squares represent the experimental line widths, and lines are the best fit to the relevant model described in the main text. Error bars on the data are contained within the markers. For panels a–c, the sample temperature is maintained at 5 K while the excitation fluence is kept at 50 nJ/cm² for measurements presented in panels d–f. Reproduced with permission from ref 13. Copyright 2019 American Physical Society.

which we have previously identified through impulsive vibrational spectroscopy. In the case of  $X_{\rm B}$  however, the phonon energy is estimated to be 21 meV with a substantially larger exciton—phonon coupling constant. 13

The phonon energy corresponding to  $X_B$  is closer to the predictions from PL line width analysis on similar material systems (see refs 4 and 7, for the analysis on (PEA)<sub>2</sub>PbI<sub>4</sub>). We note, however, that there are no LO phonon modes involving the metal-halide lattice motion at energies above 10 meV, as predicted by DFT theory and resonance Raman experiments.<sup>35</sup> There are certainly modes that correspond to the motion of the organic cation, specifically the  $\pi - \pi$  motion of the phenyl group that can be expected to have similar energies. 37,38° The mechanism that can drive the scattering of excitons that are confined within the two-dimensional metal-halide layer with uncorrelated, localized vibrations of the organic cation is, however, unclear if not physically implausible. We consider that the LO phonon scattering model is thus insufficient to explain the thermal dephasing of excitons in Ruddlesden-Popper metal halides. This is further substantiated by the failure of the model to reproduce the thermal trend of  $X_{A'}$ . We believe that the exciton polaron framework can address this discrepancy, since thermal dephasing of exciton polarons will intrinsically involve the dephasing of the phonon component of the quasi-particle through the anharmonic lattice, which is not captured by eq 3.39 We highlight that such intricacies in the scattering mechanisms cannot be reliably derived by simply performing temperaturedependent photoluminescence measurements.

**Excitation-Induced Dephasing.** The fluence dependence of the line widths over 3 orders of magnitude in the excitation densities, as shown in Figure 4, is indicative of the dominance of excitation-induced dephasing in Ruddlesden—Popper metal halides. As noted several times in this manuscript, such a dependence can never be observed in a linear PL measurement, which highlights the importance of nonlinear coherent spec-

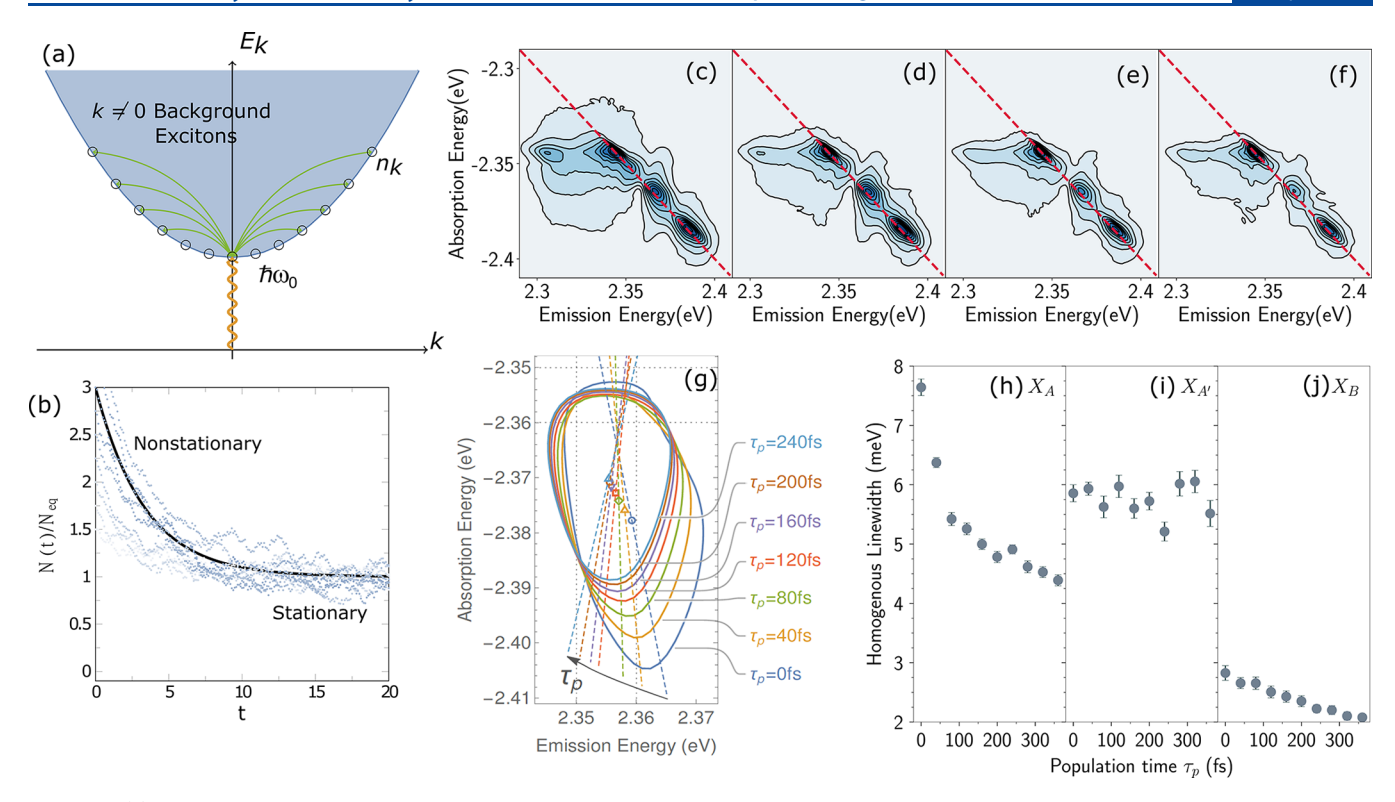


Figure 5. (a) Schematic representation of optical absorption of excitons and exciton—exciton scattering with a background population, where the dispersion relation is in the exciton representation and  $k = \vec{k}_e + \vec{k}_h$  is the exciton wavevector. (b) Time evolution of the nonstationary background population, which reaches a stationary condition asymptotically. (c)—(f) Absolute values of the experimental rephasing spectrum of (PEA)<sub>2</sub>PbI<sub>4</sub> at population waiting times of 0, 80, 160, and 240 fs, respectively, where clear narrowing of the line shape can be identified. This can also be seen more quantitatively as decreasing the homogeneous line width with the population waiting time for (h)  $X_A$  (i)  $X_{A'}$ , and (j)  $X_B$ . (g) Calculated coherent line shape contour based on the model represented in (a), which reproduces the narrowing of the line width. Reproduced with permission from ref 14. Copyright 2020 American Institute of Physics.

troscopy. The optical response function of semiconductor materials is a complex quantity, and coherent spectroscopy enables the separation of the real and imaginary components of the response function via the simultaneous measurement of the amplitude and phase.<sup>17</sup>

The linear optical absorption spectrum, measured via the transmission amplitude, corresponds to the imaginary component of the complex permittivity. A resonance in the absorption spectrum is accordingly manifested as a dispersive, first-derivative-like line shape in the real part of the linear spectrum, following the Kramers—Kronig relations. Nonlinear coherent spectroscopies can simultaneously provide both the real and imaginary components of the optical response, enabling such absorptive—dispersive line shapes to be identified in the nonlinear spectrum without the need of Kramers—Kronig analysis. When the coherent response is phased correctly, and in the absence of many-body interactions, the real part of the 2D spectrum has a symmetric absorptive line shape, while the imaginary component is dispersive.

In the presence of many-body interactions, which scramble the relative phase of the nonlinear response, the real part of the rephasing spectrum (and the nonrephasing spectrum) acquires a dispersive line shape while the imaginary component looks distinctly absorptive. Several earlier works have established such a dispersive 2D line shape as an indicator of the elastic exciton—exciton scattering through a phenomenological model based on optical Bloch equations. The model considers two distinct consequences of the Coulomb-mediated interactions between excitons: (i) excitation-induced shift in the exciton energy and

(ii) excitation-induced dephasing, which broadens the transition, both of which generate population-density-dependent terms in the time evolution of the coherence function (eq 1). Notably, this model assumes a population of excitons as the bath, which remains stationary within the dephasing time. Accordingly, while the 2D spectral intensity reduces and the line shape elongates along the diagonal due to spectral diffusion driven by energy migration, the dispersive component of the line shape remains intact during the population waiting time ( $\tau_p$ ).

In the case of (PEA)<sub>2</sub>PbI<sub>4</sub>, we have observed a very evident dispersive line shape in the real part of the rephasing spectrum at each of the three exciton resonances, <sup>14</sup> as expected from a system subject to many-body interactions (see also Figure 4a—c). The line shape, however, exhibits a very strong population—time dependence with the dispersive line shape evolving into the absorptive line shape within 500 fs. A correlated change can also be observed in the imaginary component of the response, which progressively acquires a dispersive component. These experimental observations indicate that the many-body exciton—exciton interactions are being quenched in a time scale where there is negligible loss in the population (photogenerated excitons do not recombine to the ground state withing 500 fs).

The time-evolving many-body interactions can also be observed through the absolute values ( $\sqrt{(\Re)^2 + (\Im)^2}$ ) of the rephasing spectrum shown in Figure 5c–f. The narrowing of the spectral line shape is evident in this data set, which can be further analyzed to obtain the time-dependent homogeneous line widths for the excitonic transitions,  $X_A$ ,  $X_{A'}$ , and  $X_B$ , shown in Figure 5h–j. Intriguingly, the reduction in the homogeneous

line width is very different for each of the resonances. To understand this, we must first understand the microscopic origin of the time-dependent line width.

In refs 14 and 43, we have developed a first-principles, many-body theoretical model of interacting excitons employing a quantum stochastic approach, which provides a theoretical framework in which these experimental observations can be rationalized. Our approach is similar to the Anderson—Kubo (AK) model of system—bath fluctuations, which we have elaborated upon earlier in this manuscript. The notable difference between the AK model and our treatment lies in the assumption on the nature of the stochastic bath fluctuations. Conventionally, the bath fluctuations are considered to be around a stationary state and the energy fluctuation average is around a time-independent mean value (see Figure 1a). But with the time-evolving coherence, we consider a nonstationary bath population whose relaxation is described by a stochastic equation (see Figure 5b).

The physical picture behind our model is shown in Figure 5a: at t = 0, a sequence of broadband femtosecond pulses photoexcite a nonstationary population of excitons at nonzero momenta in the exciton phase space in addition to the coherent population at k = 0. The coherent population is eventually detected via the nonlinear measurement through a very specific coherent excitation pathway, and it is the system whose spectral response is being measured. However, the energy of the coherent excitons is modulated by the Coulomb-mediated interactions with the noisy bath of the incoherent exciton population at  $k \neq 0$  with the fluctuation,  $\Delta$ , proportional to the background population density, N(t)). The fluctuations in  $\omega_{01}(t)$  in eq 1 can accordingly be derived from the fluctuations in the background population density N(t) that scatter the coherent exciton population via a many-body interaction potential. Under the Born approximation and for a finite range potential, this interaction can be described in terms of the s-wave scattering length (a) and the exciton effective mass ( $\mu$ ) as  $V_0$  =  $4\pi\hbar^2 a/\mu$ . N(t) itself is described by Ornstein-Uhlenbeck process (damped Brownian motion) that results in a the mean of the population to be  $\langle N(t) \rangle = e^{-\gamma * t} \langle N(t=) \rangle$ , where  $\gamma *$  is the background relaxation rate, as shown in Figure 5b.

Following this photophysical scenario, the optical response of function, which depends on the mean of the time-dependent coherence function in eq 1 can be shown to be proportional to<sup>43</sup>

$$\left\langle \exp\left[-i2V_0 \int_0^t N(\tau)d\tau\right]\right\rangle$$

$$= \exp[i2V_0 g_1(t)] \exp[-2V_0^2 g_2(t)], \tag{4}$$

where  $g_1(t)$  and  $g_2(t)$  are the time averaged mean and the covariance of the background population fluctuations. In simple words, they quantify the time evolution of the background population and its fluctuations. Equation 4 shows that the coherence function and accordingly the optical response oscillates at a frequency that is renormalized by  $g_1(t)$  and results in the excitation-induced shift to blue in the exciton energy. The coherence also decays at a rate determined by  $g_2(t)$ , which is faster than the intrinsic dephasing rate and density dependent and thus leads to the excitation-induced dephasing and the phase scrambling that gives rise to the dispersive line shape.

The experimental results on (PEA)<sub>2</sub>PbI<sub>4</sub>, shown in Figure 5, reveal a more dominant contribution from line narrowing and phase scrambling than from the excitation-induced shifts. This suggests a greater role from the covariance in the population

fluctuations than the overall decay in the time averaged mean. The dynamical narrowing of the rephasing spectral line shape can be reproduced within this framework, as shown in Figure 5g. The theory also predicts substantial asymmetry in the line shape along the absorption energy axis, which is clearly absent in the experimental spectrum. We attribute this again to the reduced contribution from  $g_1(t)$ . Importantly, the critical physical mechanism is not just the overall decay of the background population but the stochastic evolution of correlations in the density fluctuations, which in itself may be driven by the latticeinduced polaronic effects. Coincidentally, the time evolution of the coherent nonlinear line shape (albeit the total currelation spectrum, not resolved into the rephasing component) has also been recently observed by Kambhampati and co-workers in lead-halide nanocrystals and has been suggested to be a signature of the formation of exciton polaron.

#### PERSPECTIVE

The spectral fine structure in the optical spectra of hybrid Ruddlesden-Popper metal halides has largely been suggested to be composed of phonon replicas of a single excitonic state. We have argued that this may not be a sufficient explanation of the spectral structure based on a series of experimental observations. Two dominant resonances,  $X_A$  and  $X_B$ , can be identified within the spectral structure separated by a characteristic energy of 35 ± 5 meV. The spectral line shape can be reproduced with an empirically modified Elliott's formula, also with the Huang-Rhyss contributions, but not with phonons at 35 meV.<sup>7,45</sup> In fact, we do not observe phonons at that energy that are strongly coupled to electronic excitations in the resonance resonant impulsive stimulated Raman scattering measurement. Instead, as we elaborated in ref 35, we observe that the impulsive stimulated Raman spectra, obtained by exciting resonantly and independently the two resonances, are very distinct, implying that the  $X_{\rm A}$ and  $X_B$  are dressed by different phonons. The recombination dynamics of observed via time-resolved photoluminescence and transient absorption spectroscopies and their temperature dependence indicate nonadiabatic mixing of the excitonic states assisted by the lattice phonons, as elaborated in ref 46. The energy and sign of the biexciton binding energies of the two resonances estimated via multiquantum two-dimensional spectroscopy are very different for the two resonances and are reported in ref 32. These observations strongly suggest that these resonances correspond to distinct electronic states and are not part of single electronic manifold. There are a few recent and excellent magento absorption data<sup>38</sup> that may substantiate the vibronic assignment, and we will provide our take on those observations in a separate article.

Here, we instead highlight the lessons learned from the dephasing dynamics observed and analyzed by us in  $(PEA)_2PbI_4$ . If  $X_A$  and  $X_B$  are indeed phonon replicas, then excitation of  $X_B$  will photogenerate a phonon of 40 meV energy in addition to the excitonic state similar to that of  $X_A$ . Given that the phonon energy is an order of magnitude lower than the exciton binding energy and there is no coherent interaction/superposition of the exciton and phonon states in this picture, one would expect that the probability of many-body elastic scattering of  $X_A$  excitons will be similar, if not identical to that of  $X_B$  excitons. The experimental observation in Figure 4 indicates the contrary with evident distinctness in the dephasing rates of  $X_A$  and  $X_B$  and their temperature and fluence dependence. We already discussed the peculiarity in the thermal dephasing of these excitons and the inadequacy in the currently employed LO

phonon scattering models in this context earlier in this manuscript. We reiterate the importance of phonon—phonon interactions to properly account for the thermal dephasing mechanism (see the discussion in ref 39).

The rate of increase in the dephasing rate with increasing excitation density, albeit being in the similar order of magnitude, is considerably different for each of the resonances. The dispersive line shape and time evolution of the homogeneous line widths as shown in Figure 5 are also very evidently different for each of the resonances. Considering the stochastic scattering of the coherent exciton population with the  $k \neq 0$  excitons as the dominant dephasing mechanism, under the Born approximation, we can deduce that that the many-body interaction potential  $V_0$  is fundamentally different for  $X_A$ ,  $X_{A'}$ , and  $X_B$ . This suggests that the characteristic exciton parameters such as the swave scattering lengths (linked with the exciton size and its charge-transfer character) and the exciton effective mass are measurably different. These will not change for states that are phonon replicas of a single excitonic state. An exciting prospect here is to use the fluence and time dependence of the experimental dephasing rates to estimate the interaction potential and subsequently the scattering length scales, in the same spirit of the phase space filling models proposed by Schmitt-Rink and co-workers. <sup>47</sup> This, however, demands a more formalistic expansion of  $V_0$  beyond Born approximation and considering the exact model for the exciton polaron.

To conclude, reliable estimation of the homogeneous line widths and their dependencies on various external perturbations is crucial in quantifying exciton—bath interactions. In this Perspective, on the basis of contemporary experimental data and established theoretical models, we have argued that coherent nonlinear spectroscopy is the viable methodology to that purpose. Importantly, linear spectroscopies, while being experimentally simple, are *not* capable of providing accurate estimates of the dephasing rates. Thus, photoluminescence line widths should not be used for the estimation of electron—phonon coupling parameters of metal-halide perovskites and their derivatives.

Coherent nonlinear spectroscopies, on the other hand, not only offer the possibility to extract robust homogeneous line widths but also offer unprecedented details into the mechanistics of the many-body interactions in materials. Beyond the photon echo implementation discussed in this Perspective, other multipulse variations including the two-quantum<sup>32</sup> and zero-quantum measurements<sup>48</sup> can be unique metrologies of excitonic characteristics. Importantly, when combined with simple yet powerful theoretical models, they can be effective tools to assess the spectral density of the bath<sup>49</sup> and provide insights into the material handles to engineer it.

## AUTHOR INFORMATION

#### **Corresponding Authors**

Ajay Ram Srimath Kandada — Department of Physics and Center for Functional Materials, Wake Forest University, Winston-Salem, North Carolina 27109, United States; orcid.org/0000-0002-7420-1150; Email: srimatar@wfu.edu

Hao Li − Department of Chemistry, University of Houston, Houston, Texas 77204, United States; orcid.org/0000-0002-4234-7753; Email: hli36@central.uh.edu

Eric R. Bittner — Department of Chemistry, University of Houston, Houston, Texas 77204, United States; orcid.org/0000-0002-0775-9664; Email: ebittner@central.uh.edu

Carlos Silva-Acuña — School of Chemistry and Biochemistry, Georgia Institute of Technology, Atlanta, Georgia 30332, United States; School of Physics, Georgia Institute of Technology, Atlanta, Georgia 30332, United States; School of Materials Science and Engineering, Georgia Institute of Technology, Atlanta, Georgia 30332, United States; Departamento de Física Aplicada, Centro de Investigación y de Estudios Avanzados del Instituto Politécnico Nacional, 97310 Mérida, Yucatán, México; orcid.org/0000-0002-3969-5271; Email: carlos.silva@gatech.edu

Complete contact information is available at: https://pubs.acs.org/10.1021/acs.jpcc.2c00658

#### Notes

The authors declare no competing financial interest.

#### **Biographies**

Ajay Ram Srimath Kandada completed his Ph.D. in Physics at Politecnico di Milano (Italy) in 2013 and was a postdoctoral researcher in the Italian Institute of Technology until 2016. He was a Marie Sklodowska Curie global fellow between 2016 and 2019, during which he performed his postdoctoral research at the Université de Montréal (Canada) and at the Georgia Institute of Technology (USA). In 2020, he joined the Department of Physics at Wake Forest University, USA, as an Assistant Professor. His research interests include ultrafast optical spectroscopy of excitonic semiconductors and development of quantum optical probes of materials.

Hao Li received his Ph.D. in Physical Chemistry from Wayne State University in 2011 and was a postdoctoral researcher at the Center of Nonlinear Studies (CNLS) in Los Alamos National Laboratory until 2014. He then joined the University of Houston as a postdoctoral fellow and became a research associate since 2019. His research focuses on light—matter interactions, excited-state electronic structures, and photoexcitation dynamics in semiconductor materials.

Eric R. Bittner obtained his Ph.D. in theoretical chemistry from the University of Chicago in 1994 and subsequently was an NSF postdoctoral fellow at the University of Texas at Austin and Stanford University. In 1997, he was appointed as an Assistant Professor at the University of Houston where he is currently the Moores Professor of Chemical Physics. He is a Guggenheim and a Fulbright Fellow and holds fellowship in the APS and RSC. His research focuses upon light—matter interactions, excited state dynamics, stochastic processes, and condensed matter physics.

Carlos Silva-Acuña earned a Ph.D. in Chemical Physics from the University of Minnesota in 1998 and was then Postdoctoral Associate in the Cavendish Laboratory, University of Cambridge. In 2001 he became EPSRC Advanced Research Fellow in the Cavendish Laboratory and Research Fellow in Darwin College, Cambridge. In 2005, he joined the Université de Montréal as Assistant Professor, where he held the Canada Research Chair in Organic Semiconductor Materials from 2005 to 2015 and a Université de Montréal Research Chair from 2014 to 2017. He joined Georgia Tech in 2017, where he is currently Professor with joint appointment in the School of Chemistry and Biochemistry and the School of Physics, and Professor by Courtesy Appointment in the School of Materials Science and Engineering. He is also Honorary Professor in the Department of Applied Physics of the Centro de Investigación y de Estudios Avanzados del Instituto Politécnico Nacional (CINVESTAV Unidad Mérida). He is Fellow of the American Physical Society and the Royal Society of Chemistry. His group focuses on optical and electronic properties of organic and hybrid semiconductor materials, mainly probed by nonlinear ultrafast spectroscopies.

#### ACKNOWLEDGMENTS

This work was funded by the National Science Foundation (DMR-1904293). CS acknowledges support from the School of Chemistry and Biochemistry and the College of Science at Georgia Tech. The work at the University of Houston was funded in part by the National Science Foundation (CHE-2102506, DMR-1903785) and the Robert A. Welch Foundation (E-1337).

### REFERENCES

- (1) Mao, L.; Stoumpos, C. C.; Kanatzidis, M. G. Two-dimensional hybrid halide perovskites: principles and promises. *J. Am. Chem. Soc.* **2019**, *141*, 1171–1190.
- (2) Katan, C.; Mercier, N.; Even, J. Quantum and dielectric confinement effects in lower-dimensional hybrid perovskite semi-conductors. *Chem. Rev.* **2019**, *119*, 3140–3192.
- (3) Even, J.; Pedesseau, L.; Katan, C. Analysis of multivalley and multibandgap absorption and enhancement of free carriers related to exciton screening in hybrid perovskites. *J. Phys. Chem. C* **2014**, *118*, 11566–11572.
- (4) Gauthron, K.; Lauret, J.; Doyennette, L.; Lanty, G.; Al Choueiry, A.; Zhang, S.; Brehier, A.; Largeau, L.; Mauguin, O.; Bloch, J.; et al. Optical spectroscopy of two-dimensional layered (C<sub>6</sub>H<sub>5</sub>C<sub>2</sub>H<sub>4</sub>-NH<sub>3</sub>)<sub>2</sub>-PbI<sub>4</sub> perovskite. *Opt. Express* **2010**, *18*, 5912–5919.
- (5) Wehrenfennig, C.; Liu, M.; Snaith, H. J.; Johnston, M. B.; Herz, L. M. Homogeneous emission line broadening in the organo lead halide perovskite CH<sub>3</sub>NH<sub>3</sub>PbI<sub>3-x</sub>Cl<sub>x</sub>. *J. Phys. Chem. Lett.* **2014**, *5*, 1300–1306.
- (6) Wright, A. D.; Verdi, C.; Milot, R. L.; Eperon, G. E.; Pérez-Osorio, M. A.; Snaith, H. J.; Giustino, F.; Johnston, M. B.; Herz, L. M. Electron—phonon coupling in hybrid lead halide perovskites. *Nature Commun.* **2016**, *7*, 11755.
- (7) Neutzner, S.; Thouin, F.; Cortecchia, D.; Petrozza, A.; Silva, C.; Srimath Kandada, A. R. Exciton-polaron spectral structures in two dimensional hybrid lead-halide perovskites. *Phys. Rev. Mater.* **2018**, 2, 064605.
- (8) Ishihara, T.; Hong, X.; Ding, J.; Nurmikko, A. V. Dielectric confinement effect for exciton and biexciton states in PbI<sub>4</sub>-based two-dimensional semiconductor structures. *Surf. Sci.* **1992**, *267*, 323–326.
- (9) Lee, J.; Koteles, E. S.; Vassell, M. Luminescence linewidths of excitons in GaAs quantum wells below 150 K. *Phys. Rev. B* **1986**, 33, 5512.
- (10) Snoke, D. Solid State Physics: Essential Concepts; Addison-Wesley, 2009.
- (11) Srimath Kandada, A. R.; Petrozza, A. Photophysics of hybrid lead halide perovskites: The role of microstructure. *Acc. Chem. Res.* **2016**, *49*, 536–544.
- (12) Fuller, F. D.; Ogilvie, J. P. Experimental implementations of two-dimensional Fourier transform electronic spectroscopy. *Annu. Rev. Phys. Chem.* **2015**, *66*, 667–690.
- (13) Thouin, F.; Cortecchia, D.; Petrozza, A.; Srimath Kandada, A. R.; Silva, C. Enhanced screening and spectral diversity in many-body elastic scattering of excitons in two-dimensional hybrid metal-halide perovskites. *Phys. Rev. Rev. Res.* **2019**, *1*, 032032.
- (14) Srimath Kandada, A. R.; Li, H.; Thouin, F.; Bittner, E. R.; Silva, C. Stochastic scattering theory for excitation induced dephasing: Time-dependent nonlinear coherent exciton lineshapes. *J. Chem. Phys.* **2020**, 153, 164706.
- (15) Anderson, W. A mathematical model for the narrowing of spectral lines by exchange or motion. *J. Phys. Soc. Jpn.* **1954**, *9*, 316–339.
- (16) Kubo, R. In A stochastic theory of line shape; Shuler, K. E., Ed.; John Wiley & Sons, 1969; Vol. 15; pp 101–127.
- (17) Hamm, P.; Zanni, M. Concepts and methods of 2D infrared spectroscopy; Cambridge University Press, 2011.
- (18) Siemens, M. E.; Moody, G.; Li, H.; Bristow, A. D.; Cundiff, S. T. Resonance lineshapes in two-dimensional Fourier transform spectroscopy. *Opt. Express* **2010**, *18*, 17699–17708.
- (19) Liu, A.; Nagamine, G.; Bonato, L. G.; Almeida, D. B.; Zagonel, L. F.; Nogueira, A. F.; Padilha, L. A.; Cundiff, S. T. Toward Engineering

- Intrinsic Line Widths and Line Broadening in Perovskite Nanoplatelets. *ACS Nano* **2021**, *15*, 6499–6506.
- (20) Moody, G.; Dass, C. K.; Hao, K.; Chen, C.-H.; Li, L.-J.; Singh, A.; Tran, K.; Clark, G.; Xu, X.; Berghäuser, G.; et al. Intrinsic homogeneous linewidth and broadening mechanisms of excitons in monolayer transition metal dichalcogenides. *Nat. Commun.* **2015**, *6*, 8315.
- (21) Ni, L.; Huynh, U.; Cheminal, A.; Thomas, T. H.; Shivanna, R.; Hinrichsen, T. F.; Ahmad, S.; Sadhanala, A.; Rao, A. Real-time observation of exciton—phonon coupling dynamics in self-assembled hybrid perovskite quantum wells. *ACS Nano* **2017**, *11*, 10834—10843.
- (22) Long, H.; Peng, X.; Lu, J.; Lin, K.; Xie, L.; Zhang, B.; Ying, L.; Wei, Z. Exciton—phonon interaction in quasi-two dimensional layered (PEA)<sub>2</sub>(CsPbBr<sub>3</sub>)<sub>n-1</sub>PbBr<sub>4</sub> perovskite. *Nanoscale* **2019**, *11*, 21867—21871
- (23) Straus, D. B.; Iotov, N.; Gau, M. R.; Zhao, Q.; Carroll, P. J.; Kagan, C. R. Longer cations increase energetic disorder in excitonic 2D hybrid perovskites. *J. Phys. Chem. Lett.* **2019**, *10*, 1198–1205.
- (24) Zhang, Y.; Wang, R.; Li, Y.; Wang, Z.; Hu, S.; Yan, X.; Zhai, Y.; Zhang, C.; Sheng, C. Optical Properties of Two-Dimensional Perovskite Films of  $(C_6H_5C_2H_4NH_3)_2Pb_3I_{10}$ ]. J. Phys. Chem. Lett. **2019**, 10, 13–19.
- (25) Esmaielpour, H.; Whiteside, V.; Sourabh, S.; Eperon, G.; Precht, J.; Beard, M.; Lu, H.; Durant, B.; Sellers, I. Role of Exciton Binding Energy on LO Phonon Broadening and Polaron Formation in (BA)<sub>2</sub>PbI<sub>4</sub> Ruddlesden–Popper Films. *J. Phys. Chem. C* **2020**, 124, 9496–9505.
- (26) Peng, S.; Wei, Q.; Wang, B.; Zhang, Z.; Yang, H.; Pang, G.; Wang, K.; Xing, G.; Sun, X. W.; Tang, Z. Suppressing Strong Exciton—Phonon Coupling in Blue Perovskite Nanoplatelet Solids by Binary Systems. *Angew. Chem.* **2020**, *59*, 22156—22162.
- (27) Lao, X.; Yang, Z.; Su, Z.; Bao, Y.; Zhang, J.; Wang, X.; Cui, X.; Wang, M.; Yao, X.; Xu, S. Anomalous Temperature-Dependent Exciton—Phonon Coupling in Cesium Lead Bromide Perovskite Nanosheets. *J. Phys. Chem. C* **2019**, *123*, 5128—5135.
- (28) Saran, R.; Heuer-Jungemann, A.; Kanaras, A. G.; Curry, R. J. Giant bandgap renormalization and exciton—phonon scattering in perovskite nanocrystals. *Adv. Opt. Mater.* **2017**, *5*, 1700231.
- (29) Ghosh, S.; Śhi, Q.; Pradhan, B.; Kumar, P.; Wang, Z.; Acharya, S.; Pal, S. K.; Pullerits, T.; Karki, K. J. Phonon coupling with excitons and free carriers in formamidinium lead bromide perovskite nanocrystals. *J. Phys. Chem. Lett.* **2018**, *9*, 4245–4250.
- (30) Rubino, A.; Francisco-López, A.; Barker, A. J.; Petrozza, A.; Calvo, M. E.; Goñi, A. R.; Míguez, H. Disentangling Electron—Phonon Coupling and Thermal Expansion Effects in the Band Gap Renormalization of Perovskite Nanocrystals. *J. Phys. Chem. Lett.* **2021**, *12*, 569–575.
- (31) Yaffe, O.; Guo, Y.; Tan, L. Z.; Egger, D. A.; Hull, T.; Stoumpos, C. C.; Zheng, F.; Heinz, T. F.; Kronik, L.; Kanatzidis, M. G.; et al. Local polar fluctuations in lead halide perovskite crystals. *Phys. Rev. Lett.* **2017**. *118*. 136001.
- (32) Thouin, F.; Neutzner, S.; Cortecchia, D.; Dragomir, V. A.; Soci, C.; Salim, T.; Lam, Y. M.; Leonelli, R.; Petrozza, A.; Srimath Kandada, A. R.; et al. Stable biexcitons in two-dimensional metal-halide perovskites with strong dynamic lattice disorder. *Phys. Rev. Mater.* **2018**, *2*, 034001.
- (33) Yu, B.; Zhang, C.; Chen, L.; Huang, X.; Qin, Z.; Wang, X.; Xiao, M. Exciton linewidth broadening induced by exciton—phonon interactions in CsPbBr<sub>3</sub> nanocrystals. *J. Chem. Phys.* **2021**, *154*, 214502.
- (34) Tokmakoff, A. Two-dimensional line shapes derived from coherent third-order nonlinear spectroscopy. *J. Phys. Chem. A* **2000**, 104, 4247–4255.
- (35) Thouin, F.; Valverde-Chávez, D. A.; Quarti, C.; Cortecchia, D.; Bargigia, I.; Beljonne, D.; Petrozza, A.; Silva, C.; Srimath Kandada, A. R. Phonon coherences reveal the polaronic character of excitons in two-dimensional lead halide perovskites. *Nat. Mater.* **2019**, *18*, 349–356.
- (36) Srimath Kandada, A. R.; Silva, C. Exciton Polarons in Two-Dimensional Hybrid Metal-Halide Perovskites. *J. Phys. Chem. Lett.* **2020**, *11*, 3173–3184.

- (37) Dragomir, V. A.; Neutzner, S.; Quarti, C.; Cortecchia, D.; Petrozza, A.; Roorda, S.; Beljonne, D.; Leonelli, R.; Srimath Kandada, A. R.; Silva, C. Lattice vibrations and dynamic disorder in two-dimensional hybrid lead-halide perovskites. *arXiv:1812.05255* [cond-mat.mtrl-sci].
- (38) Urban, J. M.; Chehade, G.; Dyksik, M.; Menahem, M.; Surrente, A.; Trippe-Allard, G.; Maude, D. K.; Garrot, D.; Yaffe, O.; Delporte, E.; et al. Revealing Excitonic Phonon Coupling in  $(PE)_2(MA)_{n-1}Pb_nI_{3n+1}$  2D Layered Perovskites. *J. Phys. Chem. Lett.* **2020**, *11*, 5830–5835.
- (39) Rojas Gatjens, E.; Silva Acuña, C.; Srimath Kandada, A. R. Peculiar anharmonicity of Ruddlesden Popper metal halides: Temperature-dependent phonon dephasing. *Mater. Horiz.* **2022**, *9*, 492–499.
- (40) Shacklette, J.; Cundiff, S. T. Nonperturbative transient four-wave-mixing line shapes due to excitation-induced shift and excitation-induced dephasing. *J. Opt. Soc. Am. B* **2003**, *20*, 764–769.
- (41) Shacklette, J. M.; Cundiff, S. T. Role of excitation-induced shift in the coherent optical response of semiconductors. *Phys. Rev. B* **2002**, *66*, 045309.
- (42) Li, X.; Zhang, T.; Borca, C. N.; Cundiff, S. T. Many-Body Interactions in Semiconductors Probed by Optical Two-Dimensional Fourier Transform Spectroscopy. *Phys. Rev. Lett.* **2006**, *96*, 057406.
- (43) Li, H.; Srimath Kandada, A. R.; Silva, C.; Bittner, E. R. Stochastic scattering theory for excitation-induced dephasing: Comparison to the Anderson–Kubo lineshape. *J. Chem. Phys.* **2020**, *153*, 154115.
- (44) Sonnichsen, C. D.; Strandell, D. P.; Brosseau, P. J.; Kambhampati, P. Polaronic quantum confinement in bulk CsPb Br 3 perovskite crystals revealed by state-resolved pump/probe spectroscopy. *Phys. Rev. Res.* **2021**, *3*, 023147.
- (45) Passarelli, J. V.; Mauck, C. M.; Winslow, S. W.; Perkinson, C. F.; Bard, J. C.; Sai, H.; Williams, K. W.; Narayanan, A.; Fairfield, D. J.; Hendricks, M. P.; et al. Tunable exciton binding energy in 2D hybrid layered perovskites through donor—acceptor interactions within the organic layer. *Nature Chem.* **2020**, *12*, 672—682.
- (46) Thouin, F.; Srimath Kandada, A. R.; Valverde-Chávez, D. A.; Cortecchia, D.; Bargigia, I.; Petrozza, A.; Yang, X.; Bittner, E. R.; Silva, C. Electron-phonon couplings inherent in polarons drive exciton dynamics in two-dimensional metal-halide perovskites. *Chem. Mater.* **2019**, *31*, 7085–7091.
- (47) Schmitt-Rink, S.; Chemla, D.; Miller, D. Theory of transient excitonic optical nonlinearities in semiconductor quantum-well structures. *Phys. Rev. B* **1985**, *32*, 6601.
- (48) Liu, A.; Almeida, D.; Bae, W.; Padilha, L.; Cundiff, S. Nonmarkovian exciton-phonon interactions in core-shell colloidal quantum dots at femtosecond timescales. *Phys. Rev. Lett.* **2019**, *123*, 057403.
- (49) Liu, A.; Almeida, D. B.; Bae, W.-K.; Padilha, L. A.; Cundiff, S. T. Simultaneous existence of confined and delocalized vibrational modes in colloidal quantum dots. *J. Phys. Chem. Lett.* **2019**, *10*, 6144–6150.